RSC Advances

ROYAL SOCIETY OF CHEMISTRY

www.rsc.org/advances

Magnetic Amine Functionalized Polyacrylic Acid-Nanomagnetite for Hexavalent Chromium Removal from Polluted Water

Feng Gao, Hongbo Gu,* Huanwen Wang, Xuefeng Wang, Bo Xiang*

Shanghai Key Lab of Chemical Assessment and Sustainability, Department of Chemistry, Tongji University, Shanghai 200092, People's Republic of China

*Corresponding author

E-mail: hongbogu2014@tongji.edu.cn (H. G.), bxiangbo@tongji.edu.cn (B. X.)

Abstract

A novel magnetic amine functionalized polyacrylic acid-nanomagnetite (Fe_3O_4-PAA-NH_2) adsorbent prepared by a facile surface initiated polymerization (SIP) method has delivered a great Cr(VI) removal performance compared to as-received Fe_3O_4 nanoparticles. The maximum amine group (-NH_2) grafted onto Fe_3O_4-PAA is determined to be 3.925 mg g^{-1} based on the acid-base titrimetric analysis. The optimal pH value for Cr(VI) adsorption is around 2.0 with the Fe_3O_4-PAA-NH_2 dose of 30 mg and contact time of 10 min at room temperature. A multilayer adsorption for Freundlich isotherm model is well fitted rather than the monolayer adsorption of Langmuir isotherm model. The Cr(VI) removal kinetics by the Fe_3O_4-PAA-NH_2 nanoadsorbents is found to follow pseudo-second-order behavior with a calculated room temperature rate constant of 1.23 g mg^{-1} min^{-1} for the solution with an initial Cr(VI) concentration of 7.0 mg L^{-1} and pH value of 2.5. The competition adsorption tests show that the presence of other metals including Cu(II), Zn(II), Cd(II), K(I), Ca(II), Na(I), and Mg(II) in polluted water favors the Cr(VI) adsorption by the fabricated Fe_3O_4-PAA-NH_2 nanoadsorbents due to the affinity of the chemical potential, electronegativity of each metal element. Moreover, the prepared Fe_3O_4-PAA-NH_2 nanoadsorbents exhibit a good reusability and retain around 85% of Cr(VI) adsorption capacity even after 5 cycles.

1. Introduction

Currently, the increasing contaminations in wastewater system are the critical problems to be solved.[1, 2] Especially, the heavy metals such as chromium (Cr), cadmium (Cd), mercury (Hg), lead (Pb), and arsenic (As) are highly toxic water pollutants resulting from the industries including metal plating facilities, mining operations, fertilizer industries, tanneries, batteries, paper industries and pesticides, etc.,[3, 4] which can cause severe public health problems to animals and human beings since they can be stored, accumulated and transferred by organisms.[5] Among these heavy metal ions, hexavalent chromium (Cr(VI)) is commonly existed contaminant in the polluted water due to its extremely toxicity and notoriously mobility.[6] The U.S. Environmental Protection Agency (EPA) has set a maximum contaminant level for total Cr in drinking water is 0.1 mg L^{-1} according to the national primary drinking water regulations.[7, 8] Therefore, the rapid, efficient and economical technologies are required to be used to stringently treat the industrial wastewater before discharge in order to meet the limitations.[9] Adsorption is a traditional, favorable and feasible technique[10] to eliminate the heavy metal ions for environmental remediation due to its low cost and high efficiency.[11] In addition, adsorption can effectively remove heavy metals existed in the wastewater system at lower concentrations compared with other methods such as chemical precipitation and electrochemical methods.[12, 13]

Recently, nanostructured adsorbents have shown promising application for water decontamination owing to their high specific surface area and much more active sites than bulk materials for trapping heavy metal ions.[14, 15] However, the recycling of these nanosized adsorbents after treatment of polluted water still remains a challenge.[16]

Generally, the introduction of magnetism into nanoadsorbents can help the recycle of adsorbents from the wastewater system by directly applying an external magnetic field.[1] Meanwhile, these recycled magnetic nanoadsorbents can also be regenerated and reused for economic and practical applications. Therefore, researches start to pay attention to the design of magnetic nanoadsorbents for heavy metal remediation. For example, Kim *et al*.[16] prepared a hierarchical structured MnO_2-coated magnetite nanocomposite (Fe_3O_4/MnO_2) by a mild hydrothermal process with an maximum adsorption capacity toward Cd(II) of 53.2 mg g^{-1}. Liu *et al*.[9] fabricated a magnetic biopolymer hybrid hydrogels consisting of cellulose and chitosan as coating polymers and Fe_3O_4 as core nanoparticles from ionic liquid as solvent, which exhibited high adsorption capacities for different heavy metals (Cu(II), Fe(II), and Pb(II)). Gu *et al*.[2] reported that the magnetic Fe_3O_4-polyaniline (PANI) nanocomposites showed a unique capability to remove Cr(VI) from polluted water with a wide pH range and could be easily regenerated and reuse without decreasing the Cr(VI) removal performance.

Meanwhile, it's found that the surface functionality of adsorbents could greatly affect the adsorption of heavy metals at the interface.[17] The introduced functional groups such as carboxylate, hydroxyl, sulfate and amino groups on the adsorbent surface are responsible for the heavy metal adsorption due to their affinity with heavy metals to form the metal complexes or chelates.[18-20] Zhang *et al*.[21] reported that the thiol-functionalized multiwalled carbon nanotube/magnetite nanocomposites (CNT/Fe_3O_4) showed the maximum adsorption capacity of Hg(II) and Pb(II) are 65.52 and 65.40 mg g^{-1}, respectively. Xin *et al*.[22] noted that the amine-functionalized mesoporous Fe_3O_4 nanoparticles obtained from a hydrothermal method possessed the maximum adsorption

capacities for Pb(II), Cd(II), and Cu(II) from 369.0 to 523.6 mg g^{-1}. Qiu *et al*.[23] prepared ethyl cellulose (EC) composites modified with 20.0 wt% polyethylenimine (PEI) (PEI/ECs), which showed effective Cr(VI) removal from solutions with a wide pH range.

Based on the aforementioned advantages, this work combines the magnetism with the surface functionality together to design a novel magnetic amine-functionalized polyacrylic acid (PAA)-nanomagnetite (Fe_3O_4-PAA-NH_2) nanoadsorbents, which show the efficient Cr(VI) removal from polluted water. The PAA is introduced on the surface of Fe_3O_4 by a facile surface initiated polymerization (SIP) method in order to link the nanomagnetites with the amine groups. The presence of PAA on the surface of Fe_3O_4 can also prevent Fe3O4 from acid etching. The effects of initial Cr(VI) concentration, solution pH values and adsorbent doses on the Cr(VI) removal have been systematically investigated. The room temperature adsorption kinetics is explored by studying the Cr(VI) concentration change with the different contact times. The effect of existed other heavy metals including Cu(II), Zn(II), and Cd(II) on the adsorption of Cr(VI) and the stability of the nanoadsorbents is studied as well. The synthesized Fe_3O_4-PAA-NH_2 nanoadsorbents can reach the limitation of US EPA requirement.

2. Experimental

2.1 Materials

Acrylic acid (≥99.0%) was provided by Shanghai RichJoint Chemical Reagents Co., Ltd. Triethylene tetramine (TETA), potassium dichromate ($K_2Cr_2O_7$), nitric acid (HNO_3, 65 ~ 68 wt%), potassium nitrate (KNO_3, ≥99.0%, density: 2.109 g cm^{-3} (16 ^oC)), magnesium nitrate (hexahydrate) ($Mg(NO_3)_2 \cdot 6H_2O$, ≥99.0%, density: 1.464 g cm^{-3}), sodium nitrate ($NaNO_3$, ≥99.0%, density, 2,257 g cm^{-3}), calcium nitrate (tetrahydrate)

($Ca(NO_3)_2 \cdot 4H_2O$, ≥99.0%, density: 1.896 g cm^{-3}), zinc nitrate (hexahydrate) ($Zn(NO_3) \cdot 6H_2O$, ≥99.0%, density: 2.065 g cm^{-3}), and cupric nitrate (trihydrate) ($Cu(NO_3) \cdot 3H_2O$, 99.0 ~ 102.0%, density, 2.32 g cm^{-3}) were purchased from Sinopharm Chemical Reagent Co., Ltd. Cadmium (99.98%) was obtained from Aladdin. Ammonium persulfate (APS, $(NH_4)_2S_2O_8$, ≥98.0%) was from Chinasun Specialty Products Co. Ltd. Fe_3O_4 nanoparticles with an average size of 12 nm were obtained from Nanjing Emperor Nano Material Co., Ltd. All the chemicals were used as-received without any further treatment.

2.2 Preparation of PAA modified Fe_3O_4 nanoparticles

The PAA modified Fe_3O_4 nanoparticles (Fe_3O_4-PAA) were prepared by a SIP method. First, the Fe_3O_4 nanoparticles (2.0 g) and oxidant APS (1.0 g) were mixed in a 250 mL beaker with 100 mL deionized water for 20 minutes sonication. Then the dispersed solution was transferred into a 250 mL three-neck flask and heated to 70 ^oC in an oil bath. After that, the acrylic acid was dropped into above solution under the mechanical stirring (300 rpm) and reflux for additional 4 hours in the oil bath at 70^oC for polymerization of acrylic acid to form PAA. Finally, the product (Fe_3O_4-PAA) was vacuum filtered and washed with deionized water to remove the left oxidant and any oligomers before use for the amine-functionalization.

2.3 Fabrication of Fe_3O_4-PAA-NH_2 nanoparticles

The obtained Fe_3O_4-PAA nanoparticles were moved into a 250 mL three-neck flask and mechanically stirred in the oil bath under the reflux at 70 ^oC. The TETA with a weight ratio of 2: 1 to added acrylic acid was dropped into the above solution for further

reaction of 3 hours. The obtained powders were vacuum filtered and washed with deionized water and ethanol for several times. The final amine-functionalized Fe_3O_4-PAA-NH_2 nanocompposites were dried at 60 ^oC in an oven overnight. The preparation procedure of Fe_3O_4-PAA-NH_2 is shown in Scheme 1.

2.4 Determination of amine group content in Fe_3O_4-PAA-NH_2 nanoadsorbents

The amine group content in Fe_3O_4-PAA-NH_2 was determined by the acid-base titrimetric analysis. Around 0.1 g of Fe_3O_4-PAA-NH_2 was weighed precisely and put into a 250 mL glass conical flask which contained 50 mL deionized water and mixed with an indicator of bromocresol green-methyl red. A standard hydrochloric acid (HCl) was used to titrate above solution until the color of above solution was turned from green to colorless or red color. The amine content (C_{Amine}: mg g^{-1}) was evaluated from the following eqn (1):

$$C_{\text{Amine}} = \frac{C_{\text{HCl}} V_{\text{HCl}} M_{\text{NH}_2}}{m_{\text{Amine}}} \quad (1)$$

where C_{HCl} (mol L^{-1}) is the concentration of the standard HCl solution, V_{HCl} (L) is the volume of the consumed standard HCl solution, M_{NH_2} (g mol^{-1}) is the molecular weight of the amine group, m_{Amine} (g) is the weight of used Fe_3O_4-PAA-NH_2.

The concentration of standard HCl solution was obtained by following procedure. A 0.0052 g of anhydrous sodium carbonate (Na_2CO_3) was dissolved by the 50 mL of deionized water in a 250 mL glass conical flask with bromocresol green-methyl red as mixed indicator. The standard HCl solution was employed to titrate the Na_2CO_3 solution. As the color of solution was changed from green to red, the solution was boiled for 2 min and cooled down to the natural temperature. Then the solution was further titrated by the

standard HCl solution until the solution became colorless or red. Thus, the concentration of standard HCl solution was calculated by eqn (2):

$$C_{\mathrm{HCl}} = \frac{2 \times m_{Na_2CO_3}}{M_{Na_2CO_3} V_{\mathrm{HCl}}} \quad (2)$$

where $m_{Na_2CO_3}$ (g) is the weight of the anhydrous Na_2CO_3, $M_{Na_2CO_3}$ (g mol^{-1}) is the molecular weight of the anhydrous Na_2CO_3, V_{HCl} (L) is the volume of the consumed standard HCl solution.

2.5 Characterization of Fe_3O_4-PAA-NH_2 nanoadsorbents

The chemical structure of as-prepared nanoadsorbents was analyzed by a Fourier transform infrared spectroscopy (FT-IR, Thermo Nicolet NEXUS, Thermo Scientific) in the range of 500 to 4000 cm^{-1} with a resolution of 4 cm^{-1}. The morphologies of the synthesized nanocomposites were observed on a field emission scanning electron microscope (FE-SEM, Hitachi S-4800 system). The samples were prepared by adhering the powders onto an aluminum plate. Element mapping was carried out with an electron-probe micro-analyser (JXA-8100, JEOL). The thermalgravimetric analysis (TGA) and differential scanning calorimetry (DSC) were performed from ambient temperature to 700 °C in air condition at a heating rate of 5 °C min^{-1} using a SDT thermal-microbalance apparatus. X-ray photoelectron spectroscopy (XPS) was recorded by a Kratos AXIS Ultra DLD spectrometer using Al *Kα* (*hv* = 1486.6 eV) radiation as the excitation source under an anode voltage of 12 kV and an emission current of 10 mA. The C1s peaks were deconvoluted into the components consisting of a Gaussian line shape Lorentzian function (Gaussian = 80%, Lorentzian = 20%) on Shirley background. Brunauer–Emmett–Teller (BET) was used to measure the specific surface area of the as-prepared

nanoadsorbents. BET adsorption and desorption isotherms were obtained using a surface area analyzer (TriStar 3000, Micromeritics Instrument Corp.). The samples (around 0.1 g) were weighed and placed inside the sample holder cell. The refrigerant used was liquid nitrogen placed in a vacuum Dewar at about 77 K and the carrier gas was nitrogen. The magnetic properties of the as-received Fe_3O_4 nanoparticles, Fe_3O_4-PAA, and Fe_3O_4-PAA-NH_2 were measured on a magnetic property measurement system (Lakeshore 735 VSM Controller 7300 Series Magnetometer).

2.6 Cr(VI) removal tests

All the Cr(VI) removal tests were conducted in a 50 mL glass conical flask at room temperature. The concentration of heavy metals was determined by atomic absorption spectroscopy (AAS, Agilent 3510, USA). The reported values were the average of three measurements on each sample with a standard deviation of ±5%.

2.6.1 Effect of pH value

The pH value effect on the Cr(VI) removal by the synthesized Fe_3O_4-PAA-NH_2 was investigated by selecting solutions with a pH value of 1.0, 2.0, 3.0, 5.0, 7.0, 9.0, and 11.0, respectively. The initial pH value of Cr(VI) solutions was adjusted by NaOH (1.0 mol L^{-1}) and HCl (1 mol L^{-1}) with a pH meter (model: PHS-25C). The Fe_3O_4-PAA-NH_2 (30.0 mg) were ultrasonically (model: KQ-800KDE) dispersed in 20.0 mL solutions with initial Cr(VI) concentration of 5.4 mg L^{-1} for 10 min. Then this solution was taken out and centrifuged (model: TDL-80-2B) for Cr(VI) concentration determination. Meanwhile, the Fe_3O_4-PAA-NH_2 could also be separated from the solutions by using a permanent magnet and give the similar results.

2.6.2 Effect of initial Cr(VI) concentration

The effect of initial Cr(VI) concentration on the Cr(VI) removal was investigated by using Fe_3O_4-PAA-NH_2 (30.0 mg) to treat Cr(VI) solutions (20.0 mL) with initial Cr(VI) concentration varying from 1.3 to 7.5 mg L^{-1} for 10 min.

2.6.3 Effect of Fe_3O_4-PAA-NH_2 doses

The effect of the synthesized Fe_3O_4-PAA-NH_2 doses on the Cr(VI) removal was studied by using Fe_3O_4-PAA-NH_2 with loadings from 0.25 to 4.0 g L^{-1} to treat 20.0 mL Cr(VI) solutions with an initial Cr(VI) concentration of 7.5 mg L^{-1} and the initial pH of 3.0 for 10 min. In comparison, as-received Fe_3O_4 nanoparticles, Fe_3O_4-PAA, and Fe_3O_4-PAA-NH_2 (10.0 mg) were used to treat 20.0 mL Cr(VI) neutral solution with an initial Cr(VI) concentration of 1.0 mg L^{-1} for 5 min.

2.6.4 Isotherm study

For isotherm study, the synthesized Fe_3O_4-PAA-NH_2 (20.0 mg) nanoparticles were used to treat the different initial Cr(VI) concentrations varying from 0.5 to 4.5 mg L^{-1} with the contact time of 15 min at room temperature.

2.6.5 Kinetic study

For kinetic study, the synthesized Fe_3O_4-PAA-NH_2 (30.0 mg) were carried out to treat 20.0 mL solution with an initial Cr(VI) concentration of 7.0 mg L^{-1} and pH of 3.0 for different contact times.

2.6.6 Effect of Multi metal on the adsorption of Cr(VI) by Fe_3O_4-PAA-NH_2

To investigate the effect of other heavy metals including Cu(II), Zn(II), and Cd(II) and other metal ions such as K(I), Na(I), Ca(II), Mg(II) (which are normally existed in the real water system) in the solution on the adsorption of Cr(VI) by Fe_3O_4-PAA-NH_2, the Fe_3O_4-PAA-NH_2 (30.0 mg) was added into the multi-metal solution with the initial heavy

metal concentration of 5.0 mg L^{-1} and pH of 3.0 for 10 min treatment.

2.6.7 Regeneration of Fe_3O_4-PAA-NH_2

The Fe_3O_4-PAA-NH_2 (30.0 mg) were used to treat 20.0 mL solution with an initial Cr(VI) concentration of 5.0 mg L^{-1} for 15 min. After adsorption, the used Fe_3O_4-PAA-NH_2 nanoparticles were separated from solutions by a permanent magnet. The separated Fe_3O_4-PAA-NH_2 nanoparticles were placed into a conical flask containing 20 mL of deionized water and sonicated for 15 min for desorpion, and then separated from the solution using permanent magnet. Finally, the regenerated Fe_3O_4-PAA-NH_2 nanoparticles were dried at 60 ^oC for 3 h for reusage.

The Cr(VI) removal percentage (*R%*) is obtained by following eqn (3):

$$R\% = \frac{C_0 - C_e}{C_0} \times 100\% \quad (3)$$

where C_0 (mg L^{-1}) is the initial Cr(VI) concentration, and C_e (mg L^{-1}) is the final Cr(VI) concentration in the solution after treatment. The Cr(VI) removal capacity (q, mg g^{-1}) is quantified by eqn (4):

$$q = \frac{(C_0 - C_e)V}{m} \quad (4)$$

where V (L) represents the volume of Cr(VI) solution, m (g) stands for the mass of the used Fe_3O_4-PAA-NH_2 nanoadsorbents.

3. Results and discussion

3.1 Structure characterization of amine functionalized Fe_3O_4 nanoadsorbents

Fig. 1 illustrates the SEM microstructures of as-received Fe_3O_4 nanoparticles, Fe_3O_4-PAA, and Fe_3O_4-PAA-NH_2. The as-received Fe_3O_4 nanoparticles are ball-like morphology with an average diameter of 13.3 nm determined from Nano measure

software, Fig. 1(a), which is consistent with the information obtained from company. However, the Fe_3O_4-PAA exhibits the different morphology from the as-received Fe_3O_4 nanoparticles. The Fe_3O_4-PAA is observed to be sticky together due to the polymerized PAA on the surface of Fe_3O_4 nanoparticles, Fig. 1(b). After amino-functionalization, the Fe_3O_4-PAA-NH_2 changes into particulate again with an average diameter of 20.1 nm obtained from Nano measure software, Fig. 1(c)&(d). The increased nanoparticle diameter of Fe_3O_4-PAA-NH_2 arises from the formed PAA and amino-functionalization process.

Normally, elemental mapping of microstructures by SEM with energy dispersive X-ray spectrometry (EDS) is widely applied in science, engineering, and technology fields.[24] An element map is an image to display the 2-dimensional elements distributions in the materials. In this work, the elemental mapping is conducted on the synthesized Fe_3O_4-PAA-NH_2 to further clarify the specific components of Fe_3O_4-PAA-NH_2. Fig. 2 shows the zero loss image (a), elemental maps of (b) O, (c) C, (d) Fe, (e) N and (f) the summation of O, C, Fe, N elements. The different colors are used to represent the different elements in order to identify their compositions in the synthesized Fe_3O_4-PAA-NH_2. The presence of N element confirms the successful preparation of amino-functionalized Fe_3O_4-PAA.

Fig. 3(A) shows the FT-IR spectra of as-received Fe_3O_4 nanoparticles, Fe_3O_4-PAA, and Fe_3O_4-PAA-NH_2. The absorption peak at around 533 cm^{-1} in the as-received Fe_3O_4 nanoparticles, Fig. 3(A)-a, is attributed to the vibration of Fe-O band,[25] which shifts to 567 and 581 cm^{-1} for Fe_3O_4-PAA (Fig. 3(A)-b) and Fe_3O_4-PAA-NH_2 (Fig. 3(A)-c), respectively. In the Fe_3O_4-PAA, Fig. 3(A)-b, the strong absorption peaks at 1552 and

1710 cm^{-1} correspond to the C-O and C=O stretching vibration of carboxylic groups, respectively.[13] The peak at around 2909 cm^{-1} is related to the C-H stretching vibration on the PAA polymer backbone.[26] The peak at 3354 cm^{-1} is assigned to the O-H stretching vibration in the carboxylic groups of PAA. For the Fe_3O_4-PAA-NH_2, Fig. 3(A)-c, the peaks at around 3419 and 1320 cm^{-1} are due to the stretching vibration and bending vibration of N-H, respectively.[27] The peak at 2924 cm^{-1} is related to the C-H stretching vibration. The band at 1563 cm^{-1} (C-N stretching vibration) together with the small band at 1642 cm^{-1} (C=O stretching vibration) is the characteristic absorption peak for the formation of -CONH- groups,[13] which confirms the linkage of TETA onto the PAA polymer backbone.

Fig. 3(B) depicts the pore size distribution of as-received Fe_3O_4 nanoparticles, Fe_3O_4-PAA, and Fe_3O_4-PAA-NH_2. It's observed that the pore diameter of these three samples is wide distributed within the range of 1.5 ~ 40 nm. For the as-received Fe_3O_4 nanoparticles, the highest pore volume of 0.05297 cm^3 g^{-1} corresponds to the pore diameter of 15.1 nm. However, for the Fe_3O_4-PAA, the highest pore volume of 0.03254 cm^3 g^{-1} appears at pore diameter of 15.5 and 5.3 nm, and for the Fe_3O_4-PAA-NH_2, the highest pore volume of 0.03653 cm^3 g^{-1} corresponds to the pore diameter of 8.7 nm. These results show that the pore volume of Fe_3O_4 nanoparticles is decreased after polymerization of PAA and amino functionalization on the surface of Fe_3O_4 nanoparticles. The BET specific area of as-received Fe_3O_4 nanoparticles is measured to be 81.4216 m^2 g^{-1}, which is reduced to 61.6277, and 69.9001 m^2 g^{-1} for Fe_3O_4-PAA, and Fe_3O_4-PAA-NH_2, respectively.

Fig. 3(C)&(D) shows the TGA and DSC curves of as-received Fe_3O_4

nanoparticles, Fe_3O_4-PAA, and Fe_3O_4-PAA-NH_2 in the air condition, respectively. In the TGA curve of as-received Fe_3O_4 nanoparticles, the slight weight loss before 150 ^oC is attributed to the loss of moisture and there is no weight change after further increase temperature. This is consistent with the DSC curve of as-received Fe_3O_4 nanoparticles, in which no endothermic peak is observed during the whole procedure, Fig 3(D). However, for the Fe_3O_4-PAA, there is a significant weight loss observed around temperature range of 250 ~ 300 ^oC, which corresponds to the thermal degradation of PAA polymer chains. In DSC curve, Fig. 3(D), the thermal degradation of PAA polymer chain behaves as a sharp endothermic peak (the temperature is around 260 ^oC). Normally, the Fe_3O_4 nanparticles will get oxidized to form hematite (α-Fe_2O_3) at high temperature.[25] The weight residue of Fe_3O_4-PAA in TGA curve is determined to be 89.8% (weight percentage of α-Fe_2O_3) at 700 ^oC, which corresponds to 86.8 wt% of Fe_3O_4 nanoparticles. This means that the Fe_3O_4-PAA contains 13.2 wt% of PAA polymer. Meanwhile, the TGA profile of Fe_3O_4-PAA-NH_2 is distinct from that of the Fe_3O_4-PAA, in which two weight loss regions are observed. The weight loss from 100 to 200 ^oC is due to the elimination of the functionalized TETA small molecules on the PAA polymer backbone. The major weight loss around temperature range of 250 ~ 300 ^oC is assigned to the thermal degradation of PAA polymer backbone, which is similar to that of Fe_3O_4-PAA. Both the decomposition of TETA small molecules and PAA polymer contributes to the broad endothermic peak in the DSC curve of Fe_3O_4-PAA-NH_2, Fig. 3(D).

Fig. 3(E)&(F) shows the deconvolution of the high-resolution C1s XPS spectra of the Fe_3O_4-PAA and Fe_3O_4-PAA-NH_2, respectively. The C1s peak from the Fe_3O_4-PAA is deconvoluted into three major components with peaks at 284.9, 285.6 and 289.0 eV,

which are attributed to -CH_2-, $-\overset{|}{C}H-$, and C=O of the PAA polymer backbone, respectively, as shown in Fig. 3(E).[28] However, the C1s spectrum of Fe_3O_4-PAA-NH_2 is distinct from that of the Fe_3O_4-PAA, in which the four curves is properly fitted, Fig. 3(F). The first peak located at 285.0 eV is attributed to the aliphatic carbon of -CH_2-. The higher binding energy of 286.1 arises from the C-C of PAA and TETA. The binding energy peak located at 289.1 eV is due to the carboxylate carbon (-COOH). Most importantly, the characteristic peaks of amide (-CONH-) appears at 287.0 eV.[29] These results indicate the successful fabrication of amino functionalized Fe_3O_4-PAA nanocomposites. The amine content is determined to be 3.925 mg g^{-1} from the acid-base titrimetric analysis.

Figure 4 shows the magnetization curves of the as-received Fe_3O_4 nanoparticles and Fe_3O_4-PAA-NH_2 at room temperature. Both samples show no hysteresis loop in their magnetization curve. This means that the coercivity (H_c) is zero Oe, which indicates a superparamagnetic behavior.[30] The magnetization of both samples doesn't reach saturated at the measured magnetic field range. Therefore, the saturation magnetization (M_s) is determined by the extrapolated M_s obtained from the intercept of $M \sim H^{-1}$ at high magnetic field.[31] The M_s of the as-received Fe_3O_4 NPs is 54.47 emu g^{-1}, which is smaller than that of the bulk Fe_3O_4 (92 emu g^{-1}).[32] The obtained M_s value of Fe_3O_4-PAA-NH_2 is 47.71 emu g^{-1}. This value is sufficient for the immediate recycle of Fe_3O_4-PAA-NH_2 from solution by a permanent magnet as shown in the inset of Fig. 4. This is an essential factor in the separation and reuse of magnetic Fe_3O_4-PAA-NH_2 for the purification of water.[33] The weight percentage of Fe_3O_4 in the synthesized Fe_3O_4-PAA-NH_2 estimated from M_s value is to be around 87.0%, which is consistent with the TGA result (86.8%).

3.2 Cr(VI) removal evaluation by Fe_3O_4-PAA-NH_2 nanoadsorbents

Fig. 5(a) shows the Cr(VI) removal percentage and removal capacity from the solutions with different initial Cr(VI) concentrations at pH of 3.0 after treated with Fe_3O_4-PAA-NH_2 for 10 min. The synthesized Fe_3O_4-PAA-NH_2 with a weight of 30.0 mg is observed to be able to treat 20.0 mL solution with initial Cr(VI) concentration of 1.3 mg L^{-1} for a 100% Cr(VI) removal, which achieves the limitation of US EPA requirement. After further increasing the initial Cr(VI) concentration, the Cr(VI) removal percentage of Fe_3O_4-PAA-NH_2 decreases to 54.3% for a solution with an initial Cr(VI) concentration of 7.5 mg L^{-1}. In contrast, the Cr(VI) removal capacity increases from 0.88 to 3.31 mg g^{-1} for solutions with an initial Cr(VI) concentration changing from 1.3 to 6.5 mg L^{-1}, and then decreases to 2.70 mg g^{-1} for solutions with an initial Cr(VI) concentration of 7.5 mg L^{-1}. Normally, the active sites for the amine functionalized nanoadsorbents results from the chelation between the heavy metals and amine functional group.[34] As the gradual saturation of these active sites in the high Cr(VI) concentrations, the Fe_3O_4-PAA-NH_2 cannot accommodate the excessive Cr(VI), leading to the decreased Cr(VI) removal percentage and removal capacity as initial Cr(VI) concentration increases to 7.5 mg L^{-1}. The similar result is also observed in the carboxyl group functionalized multi-walled carbon nanotubes (MWNTs).[4]

Fig. 5(b) shows the Cr(VI) removal percentage and removal capacity with different Fe_3O_4-PAA-NH_2 doses in a 20.0 mL solution with initial Cr(VI) concentration of 7.5 mg L^{-1} and pH of 3.0 after 10 min treatment at room temperature. Both the Cr(VI) removal percentage and removal capacity are observed to increase with increasing the Fe_3O_4-PAA-NH_2 doses due to the increased active sites and amine groups for trapping

Cr(VI).[35] The Cr(VI) removal percentage increases from 21.8% for a Fe_3O_4-PAA-NH_2 dose of 0.25 g L^{-1} to 90.2% for a Fe_3O_4-PAA-NH_2 dose of 4 g L^{-1}. Meanwhile, the Cr(VI) removal capacity increases from 0.36 mg g^{-1} for a Fe_3O_4-PAA-NH_2 dose of 0.25 g L^{-1} to 24.0 mg g^{-1} for a Fe_3O_4-PAA-NH_2 dose of 4 g L^{-1}.

Fig. 5(c) shows the Cr(VI) removal percentage for the initial Cr(VI) concentration of 5.4 mg L^{-1} solutions with different pH values after treated with the Fe_3O_4-PAA-NH_2 nanoadsorbents for 10 min at room temperature. The Cr(VI) removal percentage by the Fe_3O_4-PAA-NH_2 is observed to be strongly dependent on the pH values of the solution. The Cr(VI) removal percentage increases from 61.1% for pH = 1.0 solution to 77.4% for pH = 2.0 solution and sharply decreases with increasing solution pH. The Cr(VI) removal percentage for pH = 3.0, 5.0, and 7.0 is 72.0, 41.6, 27.3%, respectively. As solution pH increase to 9.0, 10.0, 11.0, the Cr(VI) removal percentage is only around 5.9, 4.0, and 6.8%, respectively. These results demonstrate that the amine functionalized Fe_3O_4 nanoadsorbentds are not sufficient for the Cr(VI) removal as pH of solution is higher than 5, especially for the base solution. Normally, the pH dependent heavy metal removal performance is associated with both the metal chemistry in the solution and the type of the adsorbents.[36] As one of the heavy metals, the existence of Cr(VI) in solution is complicated and there are several species for Cr(VI) presented in the solutions with the different pH values. Generally, H_2CrO_4 is a strong acid, which can be ionized in the aqueous solution as shown in following eqn (5)&(6).[37]

$$H_2CrO_4 \rightleftharpoons H^+ + HCrO_4^- \qquad K_7=10^{-0.75} \tag{5}$$

$$HCrO_4^- \rightleftharpoons H^+ + CrO_4^{2-} \qquad K_8=10^{-6.45} \tag{6}$$

In the pH < 2 solution, both the H_2CrO_4 and $HCrO_4^-$ present in the solution; as pH range

is from 2 to 4, the $HCrO_4^-$ is the predominant form in the solution; when pH of solution is higher than 4, the CrO_4^{2-} starts to appear and its content is increased with increasing solution pH; as the pH of solution is above 9, the $HCrO_4^-$ disappears, only the CrO_4^{2-} exists in the solution.[38] The Cr(VI) removal performance of amine functionalized nanoadsorbents is strongly related to these existed different Cr(VI) forms. The obtained results from Fig. 5(c) indicate that the amine group prefer to chelate with the $HCrO_4^-$ ion in the solution rather than to chelate with H_2CrO_4 and CrO_4^{2-}. Therefore, the Fe_3O_4-PAA-NH_2 delivers a good Cr(VI) removal performance within the pH range of 2 ~ 3 and a poor performance after pH > 5. The proposed Cr(VI) removal mechanism is illustrated in Scheme 2. These results are consisted with the mechanism reported by Mohan *et al.*[18] They confirmed that the Cr(VI) adsorption on aminated polyacrylonitrile fibers was affected by both the electrostatic attraction and surface complexation at low solution pH values (around pH of 3.0). Mayer-Gall *et al.*[39] also reported that the amino groups are easily to protonated to form the ammonium salts in the acidic solution, which could adsorb the negatively charged chromate ion.

Fig. 5(d) illustrates the Cr(VI) removal percentage in a solution with an initial Cr(VI) concentration of 1.0 mg L^{-1} after treated with as-received Fe_3O_4 nanoparticles, Fe_3O_4-PAA, and Fe_3O_4-PAA-NH_2 (10.0 mg) in 5 min for comparison. The as-received Fe_3O_4 nanoparticles only exhibit Cr(VI) removal performance from the aqueous solution with a low removal percentage of 14.9%, which is lower than that of previous report (around 22%).[40] The Fe_3O_4-PAA also shows a poor Cr(VI) removal percentage of 15.7%. In contrast, the synthesized Fe_3O_4-PAA-NH_2 exhibits a Cr(VI) removal percentage of

55.8%, which is almost 4 times higher than as-received Fe_3O_4 nanoparticles and prepared Fe_3O_4-PAA. As-aforementioned, the BET results show that the average specific surface area for the as-received Fe_3O_4 nanoparticles, Fe_3O_4-PAA, and Fe_3O_4-PAA-NH_2 is 81.4216, 61.6277, and 69.9001 m^2 g^{-1}, respectively. Even the specific surface area decreases for the Fe_3O_4 nanoparticles after amino functionalization, the Cr(VI) removal percentage is increased. These results demonstrate that the amine group plays an important role in the Cr(VI) removal from the polluted water system. This further confirms the significance of the functional groups on the adsorbents for water treatment. The 1 mol L^{-1} HCl is used to measure the stability of as-received Fe_3O_4 nanoparticles and synthesized Fe_3O_4-PAA-NH_2 in the acidic solution. The obtained results are shown in the inset of Fig. 5(d). After immersed in the acidic solution for 1 h, the as-received Fe_3O_4 nanoparticles are observed to be dissolved in the acid solution with a formation of light brown color. However, the Fe_3O_4-PAA-NH_2 is still in the bottom of the solution and the color of solution is still clear without any changes. These results confirm that the amine functionalized Fe_3O_4-PAA nanoadsorbents are more stable in the acid solution than the as-received Fe_3O_4 nanoparticles.

From economic and practical point of view, the regeneration and reusability was investigated in this work. The Fe_3O_4-PAA-NH_2 after treated Cr(VI) solution was placed into deionized water and sonicated for 15 min for desorpion at room temperature. The regenerated Fe_3O_4-PAA-NH_2 was used to treat initial Cr(VI) concentration of 5.0 mg L^{-1} (20 mL) for 15 min. The adsorption-desorption process was conducted for 5 cycles and the obtained adsorption capacity is depicted in Fig. 6. It's observed that the adsorption capacity of Fe_3O_4-PAA-NH_2 still remains around 85% after 5th cycles, exhibiting a

relatively good reusability and stability. This indicates that the synthesized Fe_3O_4-PAA-NH_2 can be used as the reversible efficient nanoadsorbent for practical wastewater treatment.

3.3 Cr(VI) adsorption isotherm by Fe_3O_4-PAA-NH_2 nanoadsorbents

Normally, the adsorption isotherm can describe the adsorption equilibrium of adsorbate at surface of adsorbents. The adsorption equilibrium models can provide some insights to the adsorption mechanism, the surface properties and the affinity of adsorbent.[41] Two commonly used isotherm models including Langmuir and Freundlich isotherm models can explain solid-liquid adsorption systems. The Langmuir model is often used to describe the monomolecular layer adsorption, which assumes that the adsorption energy is uniformly distributed on the surface and no migration of adsorbate in the plane of surface.[42] The Langmuir model is expressed as eqn (7):

$$q_e = \frac{abC_e}{1+bC_e} \tag{7}$$

where C_e is the equilibrium concentration (mg L^{-1}) of Cr(VI), q_e is the adsorbed Cr(VI) amount at equilibrium (mg g^{-1}), a (mg g^{-1}) and b (L mg^{-1}) are Langmuir isotherm parameters. The Freundlich model is an empirical equation, which focuses on the adsorption on an energetically heterogeneous surface. The expression of Freundlich model is listed as eqn (8), which provides the relationship between the adsorbed concentration and the solute concentration:

$$q_e = k_f C_e^{\eta} \tag{8}$$

where k_f is the Freundlich equilibrium constant, indicating the extent of adsorption, and η

is the power term of the Freundlich isotherm and the heterogeneity factor, illustrating the intensity of adsorption.[43]

In order to study the adsorption equilibrium of Cr(VI) at surface of nanoadsorbents, the synthesized Fe_3O_4-PAA-NH_2 (20.0 mg) were used to treat the different initial Cr(VI) concentrations varying from 0.5 to 4.5 mg L^{-1} with the contact time of 15 min at room temperature. Both Langmuir and Freundlich isotherm models are used to fit the Cr(VI) adsorption equilibrium process by Fe_3O_4-PAA-NH_2. The obtained results are shown in Fig. 7 and te fitting parameters are listed in Table 1. According to the correlation coefficient values, the Freundlich isotherm model (R^2 = 0.976) is observed to be well fitted for the Cr(VI) adsorption by Fe_3O_4-PAA-NH_2, demonstrating a multilayer adsorption mechanism. However, the correlation coefficient values for these two models only has little difference for the Cr(VI) removal adsorption (R^2 = 0.960 for the Langmuir model). The maximum Cr(VI) adsorption capacity by Fe_3O_4-PAA-NH_2 obtained from parameter *a* of Langmuir model is 9.791 mg g^{-1}, which is higher than that of activated carbon (around 1.1 ~ 9.5 mg g^{-1})[18] and chitosan flakes (around 5.246 ~ 7.943 mg g^{-1})[44] and lower than that of magnetic carbon nanocomposites prepared from $Fe(NO_3)_3$/cellulose (15.3 mg g^{-1}),[45] chitosan-coated gauze contained amino groups (12.4 mg g^{-1}),[46] and chitosan/poly (vinyl alcohol) containing cerium(III) (52.8 mg g^{-1}).[47]

3.4 Cr(VI) removal kinetics by Fe_3O_4-PAA-NH_2 nanoadsorbents

The adsorption kinetics is one of the important parameters to describe the Cr(VI) uptake rate and control the residue time of the adsorbent at the solid-solution interface, from which the efficiency of the Cr(VI) adsorption by nanoadsorbents can be determined.[48] Therefore, the Cr(VI) removal kinetics is investigated to understand the

adsorption behavior of Cr(VI) by prepared Fe_3O_4-PAA-NH_2 nanoadsorbents. Normally, the amount of adsorbed Cr(VI) (q_t, mg g^{-1}) at time t is calculated by eqn (9):

$$q_t = \frac{(C_0 - C_t)V}{m_s} \quad (9)$$

where C_0 is the initial Cr(VI) concentration (mg L^{-1}) and C_t represents the Cr(VI) concentrations in mg L^{-1} at time t (min). The calculated q_t in solution with pH = 2.5 after treatment with Fe_3O_4-PAA-NH_2 nanoadsorbents for different contact times (3, 5, 7, 12, and 18 min) is depicted in Fig. 7. It's observed that the q_t increases as contact time reaches to 12 min and then become flat after contact time increases further to 18 min. This indicates that the adsorption of Cr(VI) by Fe_3O_4-PAA-NH_2 nanoadsorbents gradually becomes saturated as time increases to 18 min.[49] An appropriate kinetic model is required to quantify the amount changes of adsorbed Cr(VI) with time. Hence, the pseudo-second-order adsorption kinetic model is introduced to describe the Cr(VI) adsorption behavior by Fe_3O_4-PAA-NH_2 nanoadsorbents, which is expressed by eqn (10):[50]

$$\left(\frac{t}{q_t}\right) = \frac{1}{k_2 q_e^2} + \frac{t}{q_e} \quad (10)$$

where k_2 is the pseudo-second-order adsorption rate constant (g mg^{-1} min^{-1}), q_e stands for the adsorption capacity at equilibrium time (mg g^{-1}). If the pseudo-second-order adsorption kinetic model is suitable for this system, the plot of $t/q_t \sim t$ is supposed to give a linear line. And the q_e and k_2 can be calculated from the slope coefficient ($1/q_e$) and intercept ($1/k_2 q_e^2$) of the plot. The obtained corresponding kinetic plot is also shown in Fig. 8. A good linear fit of $t/q_t \sim t$ plot is observed with the fitting correlation coefficient

R^2 of 0.9996. This means that the Cr(VI) adsorption kinetics by Fe_3O_4-PAA-NH_2 nanoadsorbents obeys pseudo-second-order adsorption behavior. The obtained equilibrium adsorption capacity of q_e is 4.27 mg g^{-1} at the initial Cr(VI) concentration of 7.0 mg L^{-1}, which is consistent with the calculated q_t at 18 min is 4.22 mg g^{-1}, Fig. 8. The adsorption rate constant k_2 is calculated to be 1.23 g mg^{-1} min^{-1}, which is higher than that of chitosan/nanoclay bionanocomposites (8.763×10^{-4} g mg^{-1} min^{-1}).[51] The initial adsorption rate h (mg g^{-1} min^{-1}) at time t approaching zero is defined as eqn (11):[52]

$$h = k_2 q_e^2 \quad (11)$$

The calculated results show that the prepared Fe_3O_4-PAA-NH_2 nanoadsorbents exhibit an initial adsorption rate of 22.51 mg g^{-1} min^{-1}, which is much higher than that of magnetic graphene material (0.28 mg g^{-1} min^{-1})[6] and magnetic polypropylene nanocomposites (0.229 mg g^{-1} min^{-1}).[8]

3.5 Effect of Multi Metals on the Adsorption of Cr(VI)

Normally, many different kinds of toxic heavy metals coexist in the polluted water systems[53] and the investigation of effect of these multi metal ions on the adsorption of Cr(VI) is most important since the presence of the other heavy metal ions may possess the active sites of adsorbents and compete with each other for the adsorption sites.[54] Meanwhile, the presence of other metals such as K, Ca, Na, Mg may also influnce the adsorption process.[55] In this work, the competition adsorption of multi heavy metals including Zn(II), Cd(II), and Cu(II) in the solution with the equal initial heavy metal concentration is explored and the effect of presence of K, Ca, Na, Mg is also investigated. The obtained results are shown in Fig. 9. For the solution with Cr(VI), the Cr(VI) removal percentage is around 72%. However, for the bi-metal solutions consisting of

Cr(VI) with Zn(II), Cr(VI) with Cd(II), and Cr(VI) with Cu(II), the Cr(VI) removal percentage is 84.1, 85.2, 82.6%, respectively. For the tri-metal solutions composed of Cr(VI) with Cu(II)&Zn(II), Cr(VI) with Cu(II)&Cd(II), Cr(VI) with Cd(II)&Zn(II), the Cr(VI) removal percentage is 82.4, 80.1, and 85.6%, respectively. For the tetra-metal solution of Cr(VI), Cu(II), Zn(II), and Cd(II), the Cr(VI) removal percentage is found to be 84.2%. These results indicate that after introduction of multi heavy metal such as Cu(II), Zn(II), and Cd(II) into the solution, the Cr(VI) removal performance is increased. The presence of Cu(II), Zn(II), and Cd(II) favors the Cr(VI) adsorption by the fabricated Fe_3O_4-PAA-NH_2. The heavy metal Cd(II) is suggested to have relatively high effect on the Cr(VI) removal performance than heavy metal Zn(II) and Cu(II). The similar results are also reported by Ghorbel-Abid *et al*.[56] They found that the Cd(II) could significantly increase the adsorption capacity of Cr(VI) arising from the affinity of the chemical properties of each element (such as chemical potential, electronegativity, *et al*.). For the solution consisting of Cr(VI), K(I), Ca(II), Na(I), Mg(II), the Cr(VI) removal percentage is 60.7%. However, the Cr(VI) removal percentage is increased to 93.9% for the solution contained eight meal ions.

4. Conclusions

In this study, the Cr(VI) removal ability from polluted water by SIP method synthesized magnetic amine functionalized Fe_3O_4-PAA-NH_2 nanoadsorbents is evaluated. Even the average specific surface area of Fe_3O_4-PAA-NH_2 is lower than that of as-received Fe_3O_4 nanoparticles justified by BET results, the Cr(VI) removal percentage by Fe_3O_4-PAA-NH_2 is 4 times higher than that of as-received Fe_3O_4 nanoparticles due to the presence of amine group on the surface of Fe_3O_4-PAA-NH_2. The 30 mg of Fe_3O_4-PAA-

NH_2 nanoadsorbents is able to complete removal Cr(VI) for a 20.0 mL solution with initial Cr(VI) concentration of 1.32 mg L^{-1} after 10 min contact time, which can reach the limitation of the US EPA requirement. The Fe_3O_4-PAA-NH_2 dose of 4 g L^{-1} could remove 90.2% of Cr(VI) from 20.0 mL 7.5 mg L^{-1} Cr(VI) solution with pH of 3.0. The Cr(VI) removal percentage by the Fe_3O_4-PAA-NH_2 nanoadsorbents is observed to highly depend on the pH values of the solution and the optimal pH value for Cr(VI) removal is found in the solution with pH of 2.0. The Cr(VI) adsorption isotherm is fitted to the Freundlich isotherm model. The Cr(VI) removal kinetics by the Fe_3O_4-PAA-NH_2 nanoadsorbents obeys pseudo-second-order behavior and the calculated room temperature rate constant is 1.23 g mg^{-1} min^{-1} for the solution with an initial Cr(VI) concentration of 7.0 mg L^{-1} and pH value of 2.5. The presence of other heavy metals including Cu(II), Zn(II), Cd(II), K(I), Ca(II), Na(I), and Mg(II) in polluted water is beneficial for the Cr(VI) adsorption by the Fe_3O_4-PAA-NH_2 nanoadsorbents. Meanwhile, the prepared Fe_3O_4-PAA-NH_2 nanoadsorbents can prevent Fe_3O_4 nanoparticles from acid etching and be easily recycled from water by a permanent magnet for reuse. The prepared Fe_3O_4-PAA-NH_2 nanoadsorbents still retain around 85% of Cr(VI) adsorption performance even after 5 cycles.

Acknowledgement

The authors thank the financial support from the Science and Technology Commission of Shanghai Municipality (No. 15YF1412700) and Tongji University (No. 2014KJ028).

References

1. N. Wu, H. Wei and L. Zhang, *Environ. Sci. Technol.*, 2011, **46**, 419-425.

2. H. Gu, S. Rapole, J. Sharma, Y. Huang, D. Cao, H. A. Colorado, Z. Luo, N. Haldolaarachchige, D. P. Young, S. Wei and Z. Guo, *RSC Adv.*, 2012, **2**, 11007-11018.

3. Y. Ni, K. Mi, C. Cheng, J. Xia, X. Ma and J. Hong, *Chem. Commun.*, 2011, **47**, 5891-5893.

4. H. Gu, S. B. Rapole, Y. Huang, D. Cao, Z. Luo, S. Wei and Z. Guo, *J. Mater. Chem. A*, 2013, **1**, 2011-2021.

5. J. Gong, T. Liu, X. Wang, X. Hu and L. Zhang, *Environ. Sci. Technol.*, **45**, 6181-6187.

6. J. Zhu, S. Wei, H. Gu, S. B. Rapole, Q. Wang, Z. Luo, N. Haldolaarachchige, D. P. Young and Z. Guo, *Environ. Sci. Technol.*, 2012, **46**, 977-985.

7. D. Zhang, S. Wei, C. Kaila, X. Su, J. Wu, A. B. Karki, D. P. Young and Z. Guo, *Nanoscale*, 2010, **2**, 917-919.

8. J. Zhu, H. Gu, S. B. Rapole, Z. Luo, S. Pallavkar, N. Haldolaarachchige, T. J. Benson, T. C. Ho, J. Hopper, D. P. Young, S. Wei and Z. Guo, *RSC Adv.*, 2012, **2**, 4844-4856.

9. Z. Liu, H. Wang, C. Liu, Y. Jiang, G. Yu, X. Mu and X. Wang, *Chem. Commun.*, 2012, **48**, 7350-7352.

10. G. Zhao, J. Li, X. Ren, C. Chen and X. Wang, *Environ. Sci. Technol.*, 2011, **45**, 10454-10462.

11. K. Kadirvelu, C. Faur-Brasquet and P. L. Cloirec, *Langmuir*, 2000, **16**, 8404-8409.

12. M. A. A. Zaini, R. Okayama and M. Machida, *J. Hazard. Mater.*, 2009, **170**, 1119-1124.

13. J.-K. Yang, H.-J. Park, H.-D. Lee and S.-M. Lee, *Colloids Surf., A*, 2009, **337**, 154-158.

14. M. Fernandez-Garcia, A. Martinez-Arias, J. Hanson and J. Rodriguez, *Chem. Rev.*, 2004, **104**, 4063-4104.

15. W. Zhang, X. Shi, Y. Zhang, W. Gu, B. Li and Y. Xian, *J. Mater. Chem. A*, 2013, **1**, 1745-1753.

16. E.-J. Kim, C.-S. Lee, Y.-Y. Chang and Y.-S. Chang, *ACS Appl. Mater. Interfaces*, 2013, **5**, 9628-9634.

17. S.-J. Park and Y.-S. Jang, *J. Colloid Interface Sci.*, 2002, **249**, 458-463.

18. D. Mohan and C. U. Pittman Jr, *J. Hazard. Mater.*, 2006, **137**, 762-811.

19. D. Sud, G. Mahajan and M. Kaur, *Bioresour. Technol.*, 2008, **99**, 6017-6027.

20. B. Gao, J. Lu, R. Zhuang and G. Zhang, *J. Appl. Polym. Sci.*, 2009, **114**, 3487-3494.

21. C. Zhang, J. Sui, J. Li, Y. Tang and W. Cai, *Chem. Eng. J.*, 2012, **210**, 45-52.

22. X. Xin, Q. Wei, J. Yang, L. Yan, R. Feng, G. Chen, B. Du and H. Li, *Chem. Eng. J.*, 2012, **184**, 132-140.

23. B. Qiu, J. Guo, X. Zhang, D. Sun, H. Gu, Q. Wang, H. Wang, X. Wang, X. Zhang and B. L. Weeks, *ACS Appl. Mater. Interfaces*, 2014, **6**, 19816-19824.

24. D. E. Newbury and N. W. M. Ritchie, *J. Anal. At. Spectrom.*, 2013, **28**, 973-988.

25. J. Guo, H. Gu, H. Wei, Q. Zhang, N. S. Haldolaarachchige, Y. Li, D. P. Young, S. Wei and Z. Guo, *J. Phys. Chem. C*, 2013, **117**, 10191-10202.

26. M. Imamoglu and O. Tekir, *Desalination*, 2008, **228**, 108-113.

27. A.-N. A. El-Hendawy, *J. Hazard. Mater.*, 2009, **167**, 260-267.

28. B. C. Beard and P. Spellane, *Chemistry of Materials*, 1997, **9**, 1949-1953.

29. H. Hasar, *J. Hazard. Mater.*, 2003, **97**, 49-57.

30. H. Gu, S. Tadakamalla, Y. Huang, H. A. Colorado, Z. Luo, N. Haldolaarachchige, D. P. Young, S. Wei and Z. Guo, *ACS Appl. Mater. Interfaces*, 2012, **4**, 5613-5624.

31. Y. Li, H. Zhu, H. Gu, H. Dai, Z. Fang, N. J. Weadock, Z. Guo and L. Hu, *J. Mater. Chem. A*, 2013, **1**, 15278-15283.

32. H. Gu, Y. Huang, X. Zhang, Q. Wang, J. Zhu, L. Shao, N. Haldolaarachchige, D. P. Young, S. Wei and Z. Guo, *Polymer*, 2012, **53**, 801-809.

33. S. Li, Y. Gong, Y. Yang, C. He, L. Hu, L. Zhu, L. Sun and D. Shu, *Chem. Eng. J.*, 2015, **260**, 231-239.

34. L. Shao, X. Chang, Y. Zhang, Y. Huang, Y. Yao and Z. Guo, *Appl. Surf. Sci.*, 2013, **280**, 989-992.

35. J. Hu, C. Chen, X. Zhu and X. Wang, *J. Hazard. Mater.*, 2009, **162**, 1542-1550.

36. S. Mor, K. Ravindra and N. R. Bishnoi, *Bioresour. Technol.*, 2007, **98**, 954-957.

37. P. Mishra and R. Patel, *J. Hazard. Mater.*, 2009, **168**, 319-325.

38. K. Kadirvelu, C. Faur-Brasquet and P. L. Cloirec, *Langmuir*, 2000, **16**, 8404-8409.

39. T. Mayer-Gall, K. Opwis and J. S. Gutmann, *J. Mater. Chem. A*, 2015, **3**, 386-394.

40. P. Yuan, D. Liu, M. Fan, D. Yang, R. Zhu, F. Ge, J. Zhu and H. He, *J. Hazard. Mater.*, 2010, **173**, 614-621.

41. M. Brdar, M. Šćiban, A. Takači and T. Došenović, *Chem. Eng. J.*, 2012, **183**, 108-111.

42. R. Cheng, S. Ou, M. Li, Y. Li and B. Xiang, *J. Hazard. Mater.*, 2009, **172**, 1665-1670.

43. S. Sharma and G. P. Agarwal, *J. Colloid Interface Sci.*, 2001, **243**, 61-72.

44. Y. A. Aydin and N. D. Aksoy, *Chem. Eng. J.*, 2009, **151**, 188-194.

45. B. Qiu, H. Gu, X. Yan, J. Guo, Y. Wang, D. Sun, Q. Wang, M. Khan, X. Zhang, B. L. Weeks, D. P. Young, Z. Guo and S. Wei, *J. Mater. Chem. A*, 2014, **2**, 17454-17462.

46. F. Ferrero, C. Tonetti and M. Periolatto, *Carbohydr. Polym.*, 2014, **110**, 367-373.

47. F. Wang and M. Ge, *Text. Res. J.*, 2012, **83**, 628-637.

48. Demirbas E., Kobya M., Senturk E. and T. Ozkan, *WaterSA*, 2004, **30**, 533-539.

49. P. A. Kumar, M. Ray and S. Chakraborty, *Chem. Eng. J.*, 2009, **149**, 340-347.

50. C. Gerente, V. K. C. Lee, P. L. Cloirec and G. McKay, *Crit. Rev. Env. Sci. Technol.*, 2007, **37**, 41-127.

51. S. Pandey and S. B. Mishra, *J. Colloid Interface Sci.*, 2011, **361**, 509-520.

52. A. Gürses, Ç. Doğar, M. Yalçın, M. Açıkyıldız, R. Bayrak and S. Karaca, *J. Hazard. Mater.*, 2006, **131**, 217-228.

53. S.-Y. Wang, M.-H. Tsai, S.-F. Lo and M.-J. Tsai, *Bioresour. Technol.*, 2008, **99**, 7027-7033.

54. F. Lu, L. Gu, M. J. Meziani, X. Wang, P. G. Luo, L. M. Veca, L. Cao and Y. P. Sun, *Adv. Mater.*, 2009, **21**, 139-152.

55. S. Yalçin and R. Apak, *Anal. Chim. Acta*, 2004, **505**, 25-35.

56. I. Ghorbel-Abid and M. Trabelsi-Ayadi, *Arabian J. Chem.*, 2015, **8**, 25-31.

Table 1 Langmuir and Freundlich adsorption isotherm parameters.

	Langmuir			Freundlich		
Parameter	a (mg g^{-1})	b (Lmg^{-1})	R^2	k_f (mg$^{1-\eta}$L$^{\eta}$g^{-1})	η	R^2
Value	9.791	0.074	0.960	0.731	0.799	0.976

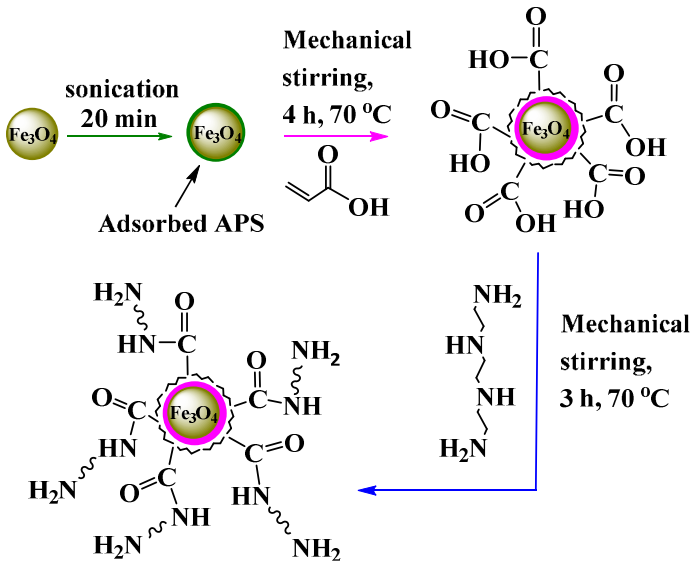

Scheme 1 Preparation procedure of Fe_3O_4-PAA-NH_2.

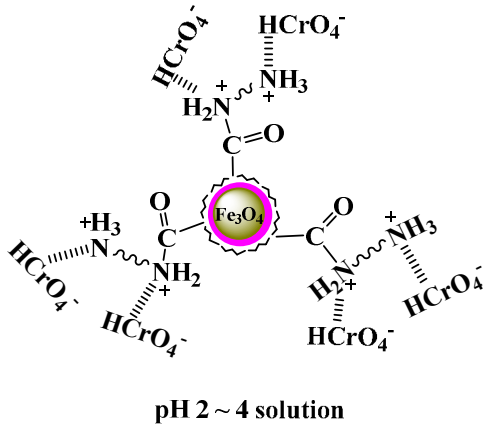

Scheme 2 Proposed adsorption of Cr(VI) species on Fe_3O_4-PAA-NH_2 in the pH of 2 ~ 4 solution.

Figure and Figure Captions:

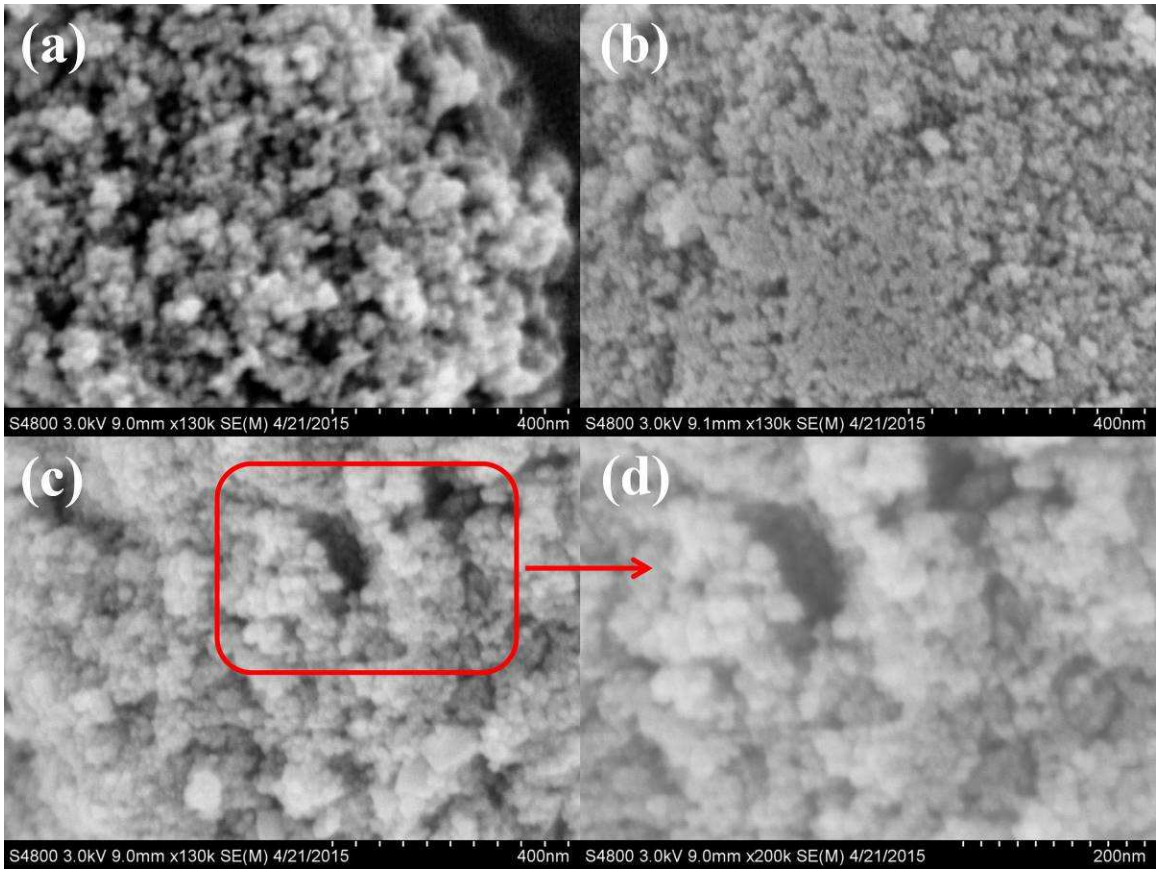

Fig. 1 SEM micrographs of (a) as-received Fe_3O_4 nanoparticles, (b) Fe_3O_4-PAA, (c) Fe_3O_4-PAA-NH_2, and (d) enlarged picture of Fe_3O_4-PAA-NH_2 nanoadsorbents.

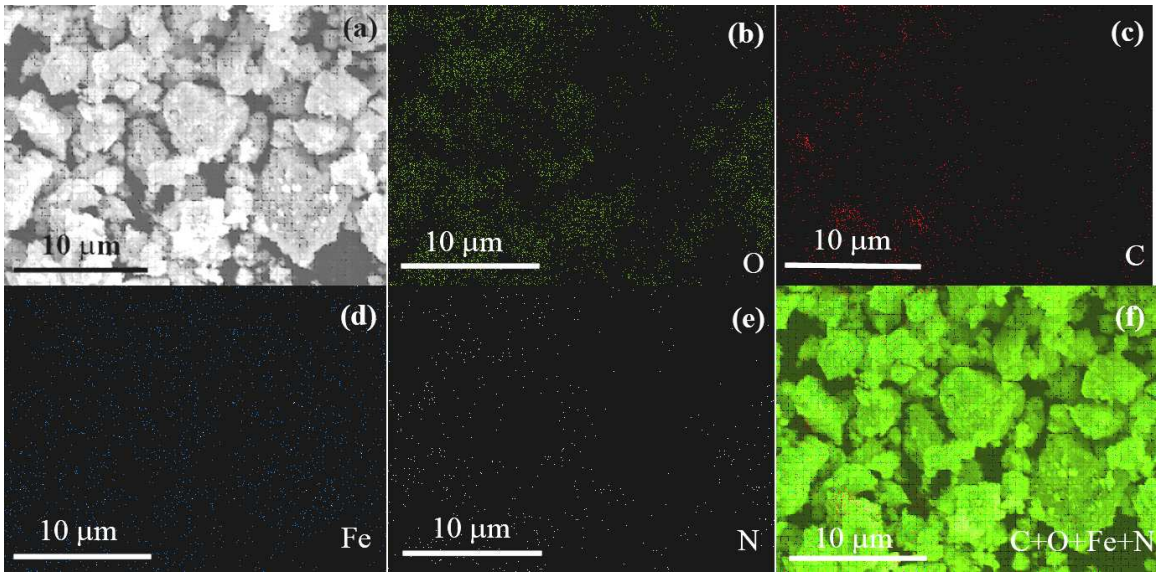

Fig. 2 SEM elemental mapping photographs of (a) Fe_3O_4-PAA-NH_2 nanoparticles, (b) O map, (c) C map, (d) Fe map, (e) N map, and (f) C+O+Fe+N map.

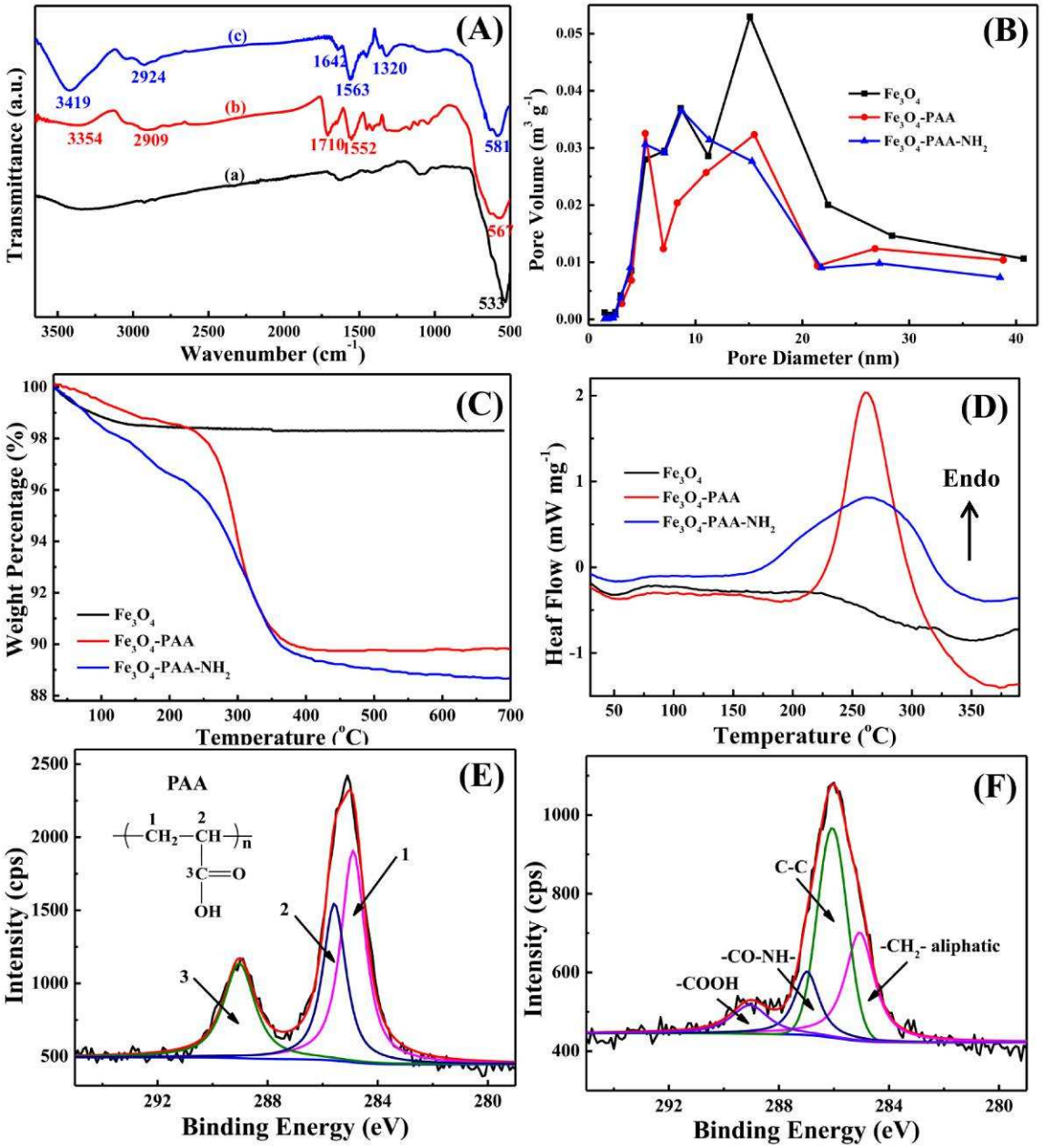

Fig. 3 (A) FT-IR spectra of (a) as-received Fe_3O_4 nanoparticles, (b) Fe_3O_4-PAA, (c) Fe_3O_4-PAA-NH_2; (B) Pore size distribution of as-received Fe_3O_4 nanoparticles, Fe_3O_4-PAA, and Fe_3O_4-PAA-NH_2; (C) TGA curves, (D) DSC curves of as-received Fe_3O_4 nanoparticles, Fe_3O_4-PAA, and Fe_3O_4-PAA-NH_2; high resolution C1s XPS spectra of (E) Fe_3O_4-PAA, and (F) Fe_3O_4-PAA-NH_2.

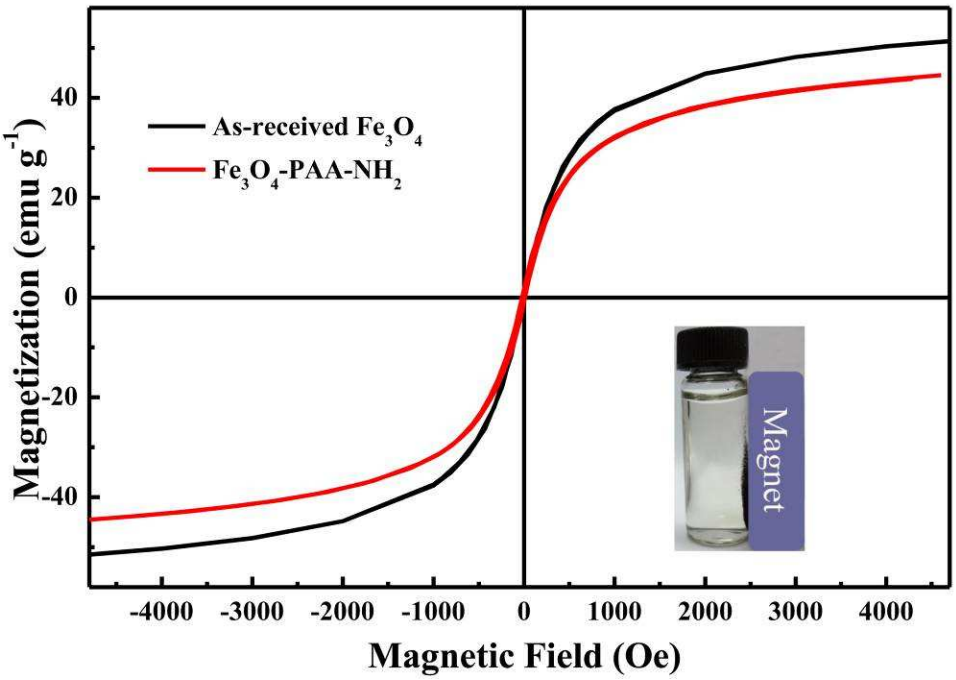

Fig. 4 Magnetization curves of as-received Fe_3O_4 nanoparticles and Fe_3O_4-PAA-NH_2. Inset shows the Fe_3O_4-PAA-NH_2 can be attracted by a permanent magnet.

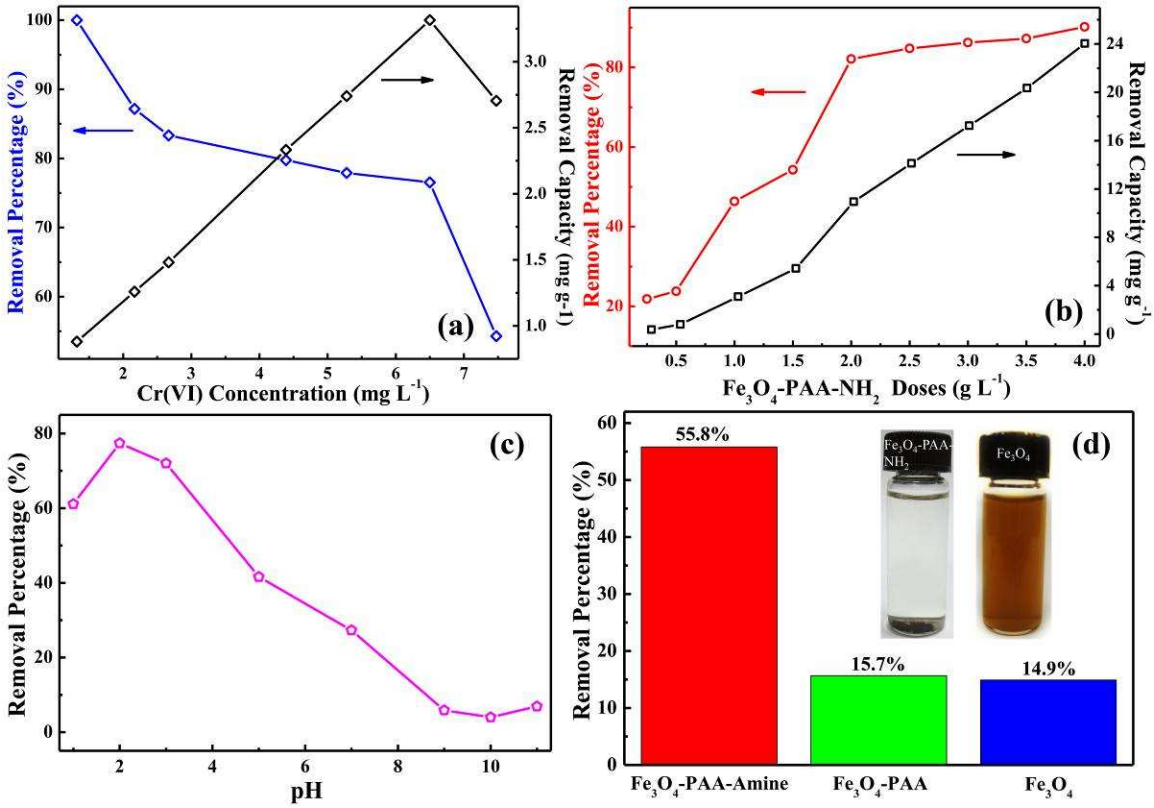

Fig. 5 (a) Removal percentage and removal capacity of 30.0 mg Fe_3O_4-PAA-NH_2 for 20.0 mL Cr(VI) solutions with different initial Cr(VI) concentrations after 10 min contact time at pH of 3.0 at room temperature; (b) removal percentage and removal capacity of different Fe_3O_4-PAA-NH_2 doses for 20.0 mL Cr(VI) solution with an initial concentration of 7.5 mg L^{-1} and pH of 3.0 after 10 min contact time at room temperature; (c) removal percentage of 30 mg Fe_3O_4-PAA-NH_2 for different pH values of 20.0 mL Cr(VI) solutions with an initial concentration of 5.4 mg L^{-1} after 10 min contact time at room temperature; (d) removal percentage comparison of 10.0 mg Fe_3O_4-PAA-NH_2, Fe_3O_4-PAA, and as-received Fe_3O_4 nanoparticles treated with 20.0 mL Cr(VI) solution with initial Cr(VI) concentration of 1.0 mg L^{-1} after 5 min contact time. The inset is Fe_3O_4-PAA-NH_2 nanoadsorbents and as-received Fe_3O_4 nanoparticles after immersed in the 1.0 mol L^{-1} HCl for one hour.

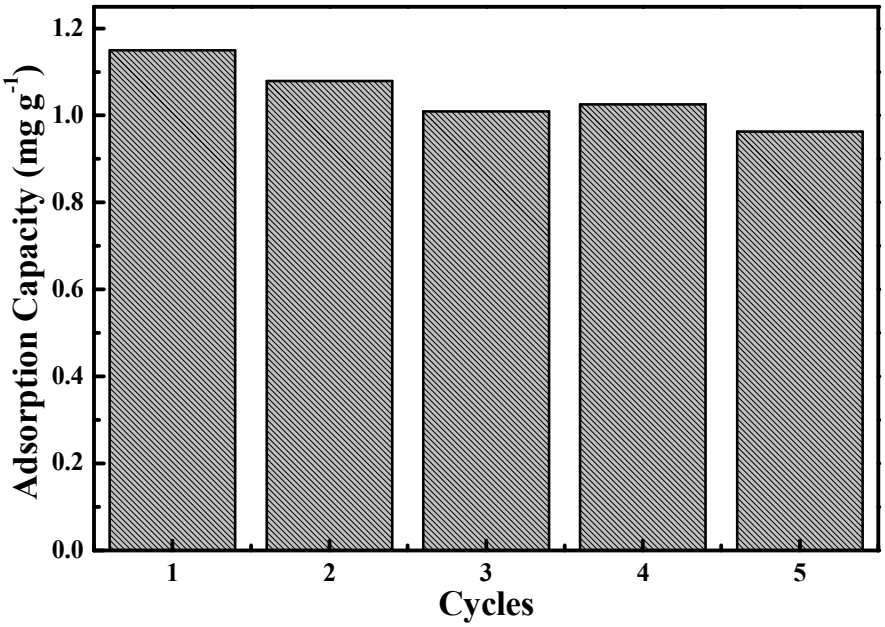

Fig. 6 Cr(VI) adsorption capacity of the regenerated Fe_3O_4-PAA-NH_2 in the 20 mL of initial Cr(VI) concentration of 5.0 mg L^{-1} with the contact time of 15 min.

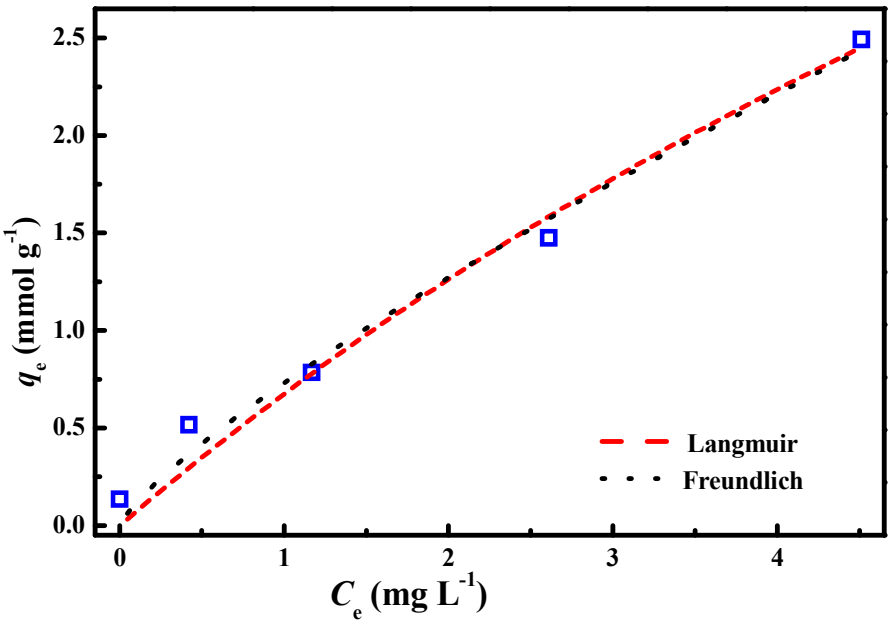

Fig. 7 Adsorption isotherm of 20.0 mL Cr(VI) solution (5 mg L^{-1}) on Fe_3O_4-PAA-NH_2 (20 mg) for 15 min contact time at room temperature.

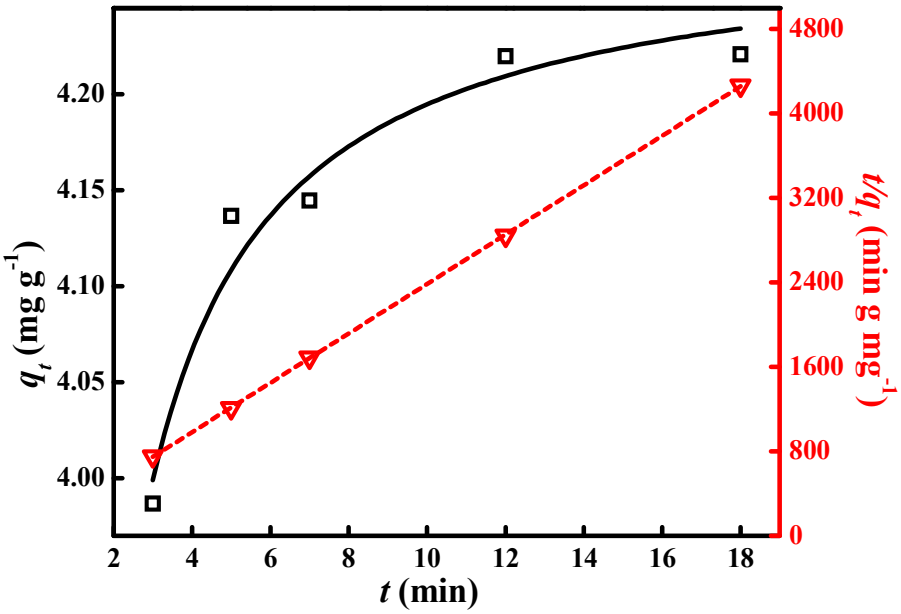

Fig. 8 Cr(VI) removal rate q_t *vs*. t for 30.0 mg Fe_3O_4-PAA-NH_2 after treated with 20.0 mL Cr(VI) solution (7.0 mg L^{-1}) under different contact times at room temperature (square line), and corresponding kinetic plot (circle line).

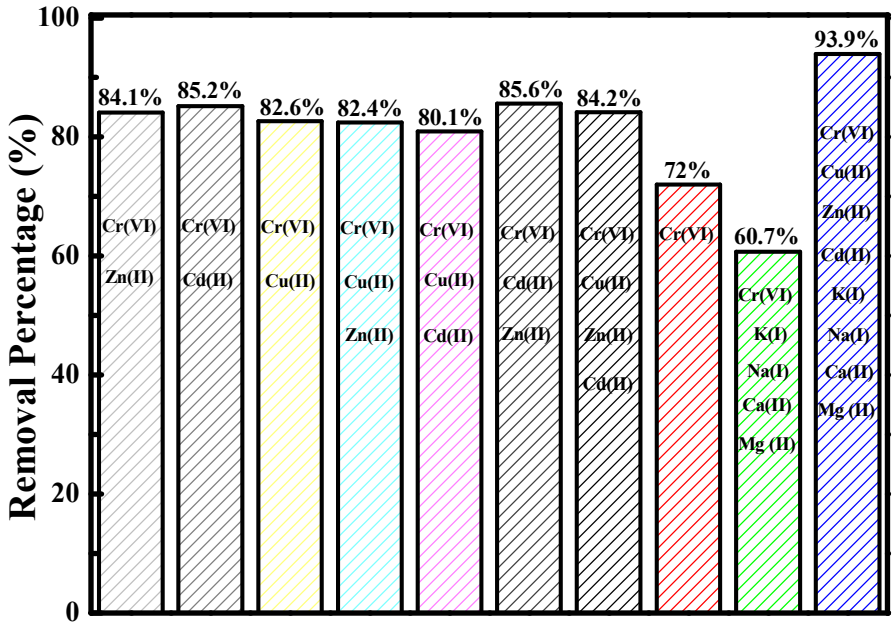

Fig. 9 Cr(VI) removal percentage in the multi-metal solution including Cr(VI), Cu(II), Zn(II), and Cd(II) with an equal initial concentration of 5.0 mg L^{-1} and pH of 3.0 after treatment of 10 min by 30 mg Fe_3O_4-PAA-NH_2.

Table of Contents

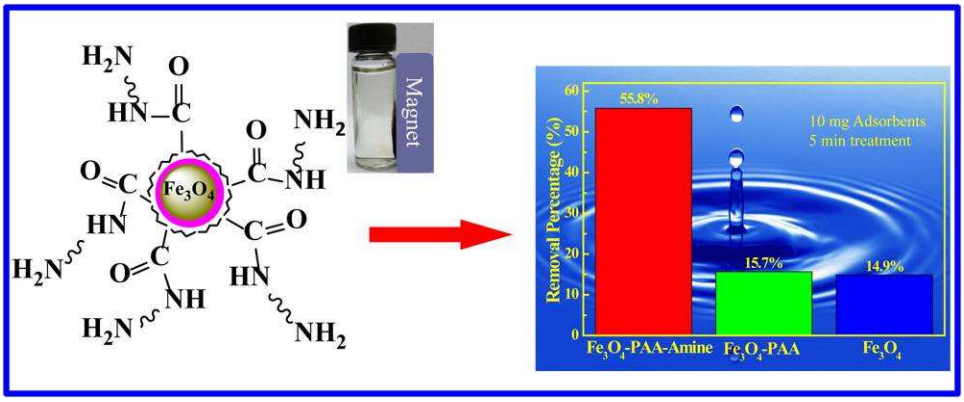

The magnetic amine functionalized polyacrylic acid-nanomagnetite adsorbents are developed for the toxic hexavalent chromium removal from polluted water.